

Constraining the neutrino mass using a multi-tracer combination of two galaxy surveys and CMB lensing

Mario Ballardini^{1,2,3,4*}, Roy Maartens^{4,5,6}

¹Dipartimento di Fisica e Astronomia, Alma Mater Studiorum Università di Bologna, via Gobetti 93/2, I-40129 Bologna, Italy

²INAF/OAS Bologna, via Piero Gobetti 101, I-40129 Bologna, Italy

³INFN, Sezione di Bologna, via Irnerio 46, I-40126 Bologna, Italy

⁴Department of Physics & Astronomy, University of the Western Cape, Cape Town 7535, South Africa

⁵Institute of Cosmology & Gravitation, University of Portsmouth, Portsmouth PO1 3FX, UK

⁶National Institute of Theoretical & Computational Sciences (NITeCS), South Africa

29 November 2021

ABSTRACT

Measuring the total neutrino mass is one of the most exciting opportunities available with next-generation cosmological data sets. We study the possibility of detecting the total neutrino mass using large-scale clustering in 21cm intensity mapping and photometric galaxy surveys, together with CMB information. We include the scale-dependent halo bias contribution due to the presence of massive neutrinos, and use a multi-tracer analysis in order to reduce cosmic variance. The multi-tracer combination of an SKAO-MID 21cm intensity map with Stage 4 CMB dramatically shrinks the uncertainty on total neutrino mass to $\sigma(M_\nu) \simeq 45$ meV, using only linear clustering information ($k_{\max} = 0.1 h/\text{Mpc}$) and without a prior on optical depth. When we add to the multi-tracer the clustering information expected from LSST, the forecast is $\sigma(M_\nu) \simeq 12$ meV.

Key words: cosmological parameters – large-scale structure of Universe – cosmic background radiation – neutrinos

1 INTRODUCTION

Massive neutrinos leave unique imprints on cosmological observables throughout the history of the Universe (see Hannestad 2006; Lesgourgues & Pastor 2006; Wong 2011; Lesgourgues & Pastor 2012; Lattanzi & Gerbino 2018, for reviews). As a result, cosmology is likely to deliver the first experimental measurement of the total neutrino mass $M_\nu \equiv \sum m_\nu$.

Cosmological data from *Planck* 2018 (Planck Collaboration, 2020a,c) in combination with BOSS DR12 clustering information (BOSS Collaboration, 2017), currently provide the constraint $M_\nu < 120$ meV at 95% confidence level (CL) (Planck Collaboration, 2020b; Vagnozzi et al. 2017; Ivanov et al. 2020). The current best neutrino mass limit is $M_\nu < 90$ meV (95% CL) (Di Valentino et al. 2021), which uses also the additional information from Pantheon Type Ia supernovae and eBOSS DR16 cosmological measurements.

These limits are model-dependent and usually weaken in cosmologies beyond the Λ CDM+ M_ν model, in particular for cosmologies with extended dark energy models or modified theories of gravity (Vagnozzi et al. 2017; Roy Choudhury & Hannestad 2020; Ballardini et al. 2020; Sekiguchi & Takahashi 2021).

On the other hand, future cosmic microwave background (CMB) anisotropy observations from ground-based experiments and satellites, such as CMB-S4¹, LiteBIRD² and the Simons Observatory³, together with large-scale structure surveys that will be performed

by DESI⁴, Euclid⁵, Roman Space Telescope⁶, Rubin Observatory⁷, SKA Observatory⁸, and others, promise a robust detection of the cosmological neutrino mass also for extended models (Allison et al. 2015; Villaescusa-Navarro et al. 2015; Schmittfull & Seljak 2018; Sprenger et al. 2019; Brinckmann et al. 2019; Yu et al. 2018; Boyle 2019).

Neutrinos can travel cosmological distances during structure formation, modifying halo formation on large scales and inducing scale-dependence of the halo bias around the neutrino free-streaming scale. This changes the relation between the halo number density and the matter (CDM+baryon) density contrast. The effect was predicted by Villaescusa-Navarro et al. (2014); Castorina et al. (2014); LoVerde (2014), and measured in N-body simulations by Villaescusa-Navarro et al. (2014) and Chiang et al. (2018, 2019).

LoVerde (2016) proposed a very promising way to target the detection of the cosmological neutrino mass using the so-called *multi-tracer* approach (Seljak 2009) and focusing on this scale-dependent feature in the halo bias. Halo bias is particularly interesting because it is a quantity that is not subject to cosmic variance when combining the information coming from different tracers of large-scale structure.

While the importance of the scale-dependent bias due to massive neutrinos and its consequences for parameter inference has been

* Contact e-mail: mario.ballardini@inaf.it

¹ <https://cmb-s4.org>

² <http://litebird.jp>

³ <https://simonsobservatory.org>

⁴ <https://www.desi.lbl.gov>

⁵ <https://www.euclid-ec.org>

⁶ <https://wfirst.gsfc.nasa.gov>

⁷ <https://www.lsst.org>

⁸ <https://www.skatelescope.org>

investigated and stressed in [Raccanelli et al. \(2019\)](#) and [Vagnozzi et al. \(2018\)](#), in our work we investigate the possibility to improve the neutrino mass measurement through the combination and cross-correlation of radio, optical, and microwave cosmological observations.

This paper is organized as follows: in [section 2](#) we briefly review the scale-dependent features imprinted on the halo bias in cosmologies with massive neutrinos. We summarize the key specifications for the radio (SKAO-MID Band 1 and the futuristic PUMA 21cm intensity mapping), optical (LSST), and microwave (CMB-S4) surveys considered in our analysis in [section 3](#). We discuss the cross-correlation coefficient between CMB lensing and large-scale structure clustering in [section 4](#). Finally, we present our results in [section 5](#) and we draw our conclusions in [section 6](#).

2 SCALE-DEPENDENT BIAS FROM MASSIVE NEUTRINOS

On very large scales, there is a linear relationship between fluctuations in the number density of halos, $\delta_h \equiv \delta n_h / n_h$, and fluctuations in the underlying density field, $\delta_X \equiv \delta \rho_X / \rho_X$ ([LoVerde 2014](#)):

$$\delta_h = b \delta_X , \quad (1)$$

where X denotes baryons (b), cold dark matter (CDM, c), massive neutrino (ν), or a combination of them.

On scales above the baryonic Jeans scale, baryons and CDM behave indistinguishably and can be treated as a single fluid, with energy density $\rho_{bc} \equiv \rho_b + \rho_c$, and number density contrast

$$\delta_{bc} = \frac{\Omega_b \delta_b + \Omega_c \delta_c}{\Omega_b + \Omega_c} . \quad (2)$$

The halo bias defined with respect to the CDM + baryon fluid,

$$b_{bc} = \frac{\delta_h}{\delta_{bc}} , \quad (3)$$

is scale independent on large scales and universal, since halo formation is governed by local processes only ([Kaiser 1984; Bardeen et al. 1986; Coles 1993; Mann et al. 1998](#)). Scale-dependent features might arise due to properties inherited in galaxy formation and evolution, and they naturally appear on small scales ([Castorina et al. 2014](#)).

If we define the halo bias relative to the total matter field

$$b_m = \frac{\delta_h}{\delta_m} , \quad (4)$$

where

$$\delta_m = \frac{\Omega_{bc} \delta_{bc} + \Omega_\nu \delta_\nu}{\Omega_m} = (1 - f_\nu) \delta_{bc} + f_\nu \delta_\nu , \quad (5)$$

then this manifests a scale-dependent feature from massive neutrinos, with a step-like behaviour, around the neutrino free-streaming scale ([Eisenstein & Hu 1997; Hu & Eisenstein 1998; Castorina et al. 2014; Villaescusa-Navarro et al. 2014; LoVerde 2014](#)). This is illustrated in [Figure 1](#).

On scales larger than the neutrino free-streaming scale, and when neutrinos are non-relativistic, the bc and ν fluids are tightly coupled, $\delta_{bc} \approx \delta_\nu$, leading to $\delta_m \approx \delta_{bc}$. On smaller scales, neutrino perturbations are damped and neutrinos do not cluster, so that $\delta_m \approx (1 - f_\nu) \delta_{bc}$. The amplitude of the feature is larger in cosmologies with larger neutrino masses (see [Figure 1](#)), and for more massive halos ([LoVerde 2014; Raccanelli et al. 2019](#)).

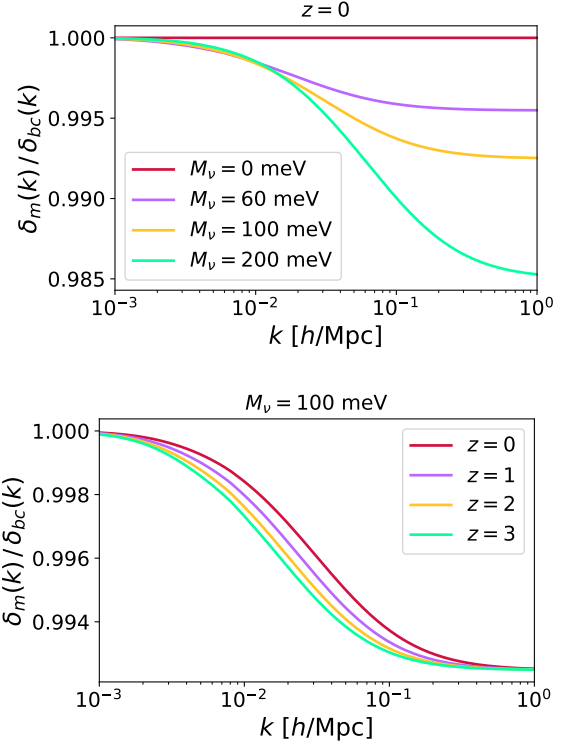


Figure 1. Scale-dependence induced in the matter density contrast in the presence of a single massive neutrino. *Top:* At $z = 0$, with $M_\nu = 0, 60, 100, 200$ meV. *Bottom:* With $M_\nu = 100$ meV, at $z = 0, 1, 2, 3$.

3 METHODOLOGY AND SIMULATED DATASETS

Following [Ballardini et al. \(2019\)](#), we use the Fisher matrix formalism to forecast constraints on the cosmological parameters, assuming that the observed fields are Gaussian random distributed.

The Fisher matrix at the power spectrum level is then

$$F_{\alpha\beta} = f_{\text{sky}} \sum_{\ell=\ell_{\min}}^{\ell_{\max}} \left(\frac{2\ell+1}{2} \right) \text{tr}[\mathbf{C}_{\ell,\alpha} \boldsymbol{\Gamma}_\ell^{-1} \mathbf{C}_{\ell,\beta} \boldsymbol{\Gamma}_\ell^{-1}] , \quad (6)$$

where $\mathbf{C}_\ell = [\mathbf{C}_\ell(z_i, z_j)]$ is the covariance matrix, $\mathbf{C}_{\ell,\alpha} = \partial \mathbf{C}_\ell / \partial \theta_\alpha$ is its derivative with respect to the cosmological parameter θ_α , and $\boldsymbol{\Gamma}_\ell = \mathbf{C}_\ell + \mathbf{N}_\ell$ is the observed covariance, with \mathbf{N}_ℓ the diagonal noise matrix. This equation assumes that all experiments observe the same patch of sky, with the same f_{sky} .

We consider for each experiment its own sky fraction, while for the cross-correlations we use the estimated overlapping sky fractions. In particular, we assume $f_{\text{sky}} = 0.4$ for CMB-S4, $f_{\text{sky}} \approx 0.48$ for SKAO-MID, $f_{\text{sky}} = 0.5$ for PUMA, $f_{\text{sky}} \approx 0.33$ for LSST, and $f_{\text{sky}} = 0.4$ for CMB-S4 \times SKAO-MID, $f_{\text{sky}} = 0.4$ for CMB-S4 \times PUMA, $f_{\text{sky}} \approx 0.33$ for CMB-S4 \times LSST, $f_{\text{sky}} \approx 0.33$ for SKAO-MID \times LSST, $f_{\text{sky}} \approx 0.33$ for PUMA \times LSST. We calculate the Fisher matrices over the common patch and then we add them together.

The angular power spectra are

$$C_\ell^{XY}(z_i, z_j) = 4\pi \int \frac{dk}{k} \mathcal{P}_R(k) I_\ell^X(k, z_i) I_\ell^Y(k, z_j) . \quad (7)$$

Here $X, Y = T, E, \phi$ for the CMB, and $= \Delta_g$ or Δ_{HI} for the galaxy or intensity mapping (IM) surveys of post-reionisation neutral hydrogen (HI), where $\Delta_g = \delta_g +$ observational corrections from observing on the past lightcone, and similarly for Δ_{HI} (see [Challinor & Lewis 2011](#);

Alonso et al. 2015; Alonso & Ferreira 2015; Fonseca et al. 2015; Ballardini & Maartens 2019; Ballardini et al. 2019, for details). \mathcal{P}_R is the dimensionless primordial power spectrum and the large-scale structure kernels are

$$I_\ell^{\Delta g}(k, z_i) = \int dz n_g^i(z) \Delta_\ell^g(k, z), \quad (8)$$

$$I_\ell^{\Delta HI}(k, z_i) = \int dz W_{\text{th}}(z, z_i) \bar{T}_{\text{HI}}(z) \Delta_\ell^{\Delta HI}(k, z), \quad (9)$$

where $\Delta_\ell^g, \Delta_\ell^{\Delta HI}$ are the angular transfer functions (Ballardini & Maartens 2019), and $W_{\text{th}}(z, z_i)$ is a smoothed top-hat window function for the i -th bin to ensure numerical stability. $n_g(z_i)$ includes a Gaussian window over the average angular number density \bar{n}_g (see below), and \bar{T}_{HI} is the average brightness temperature. We refer the reader to Hu & White (1997) for the details of the CMB temperature and polarization window functions.

The standard cosmological parameter vector that we use is

$$\theta = \left\{ \omega_b, \omega_c, H_0, \tau, \ln(10^{10} A_s), n_s, M_\nu \right\}. \quad (10)$$

We also include a pair of nuisance parameters for each redshift bin, in each of the large-scale structure surveys, allowing for a free redshift evolution of the clustering bias b_g , or of the combination $\bar{T}_{\text{HI}} b_{\text{HI}}$ for IM, and for a free redshift evolution of the galaxy magnification bias s_g .

The fiducial cosmology used for the standard cosmological parameters follows *Planck* 2018 (Planck Collaboration, 2020b): $\omega_b = 0.022383$, $\omega_c = 0.12011$, $H_0 = 67.32$ km/s/Mpc, $\tau = 0.0543$, $\ln(10^{10} A_s) = 3.0448$, $n_s = 0.96605$, $M_\nu = 60$ meV. We assume one massive and two massless neutrinos with $N_{\text{eff}} = 2.046$. All angular power spectra are calculated using a modified version of the publicly available code⁹ CAMB (Lewis et al. 2000; Howlett et al. 2012; Challinor & Lewis 2011). Small-scale non-linear corrections to the matter power spectrum are modelled with the Halofit model (Bird et al. 2012; Takahashi et al. 2012).

3.1 Radio survey: single-dish mode

We consider intensity maps of the 21cm emission of neutral hydrogen. For the fiducial linear bias model and background HI brightness temperature, we use the fitting formulas (MeerKCLASS Collaboration, 2017):

$$b_{\text{HI}}(z) = 0.667 + 0.178 z + 0.0502 z^2, \quad (11)$$

$$\bar{T}_{\text{HI}}(z) = 0.0559 + 0.232 z - 0.0241 z^2 \text{ mK}. \quad (12)$$

The noise variance for IM with N_{dish} dishes in single-dish mode in the frequency i -channel, assuming scale-independence and no correlation between the noise in different frequency channels, is (Knox 1995; Bull et al. 2015; Durrer et al. 2020; Jolicoeur et al. 2021)

$$\sigma_{\text{HI}}(v_i) = \frac{4\pi f_{\text{sky}} T_{\text{sys}}^2(v_i)}{2N_{\text{dish}} t_{\text{tot}} \Delta v}, \quad (13)$$

$$T_{\text{sys}}(v_i) = 25 + 60 \left(\frac{300 \text{ MHz}}{v_i} \right)^{2.55} \text{ K}, \quad (14)$$

where t_{tot} is the total observing time. We assume the noise is deconvolved with a Gaussian beam, modelled as

$$N_\ell^{\Delta HI}(v_i) = \sigma_{\text{HI}}(v_i) B_\ell^{-2}(v_i), \quad (15)$$

⁹ <https://github.com/cmbant/CAMB>

with

$$B_\ell = \exp \left[-\ell(\ell+1) \frac{\theta_{\text{FWHM}}^2}{16 \ln 2} \right], \quad (16)$$

and

$$\theta_{\text{FWHM}} = \frac{1.22 \lambda_i}{D_{\text{dish}}} \quad \text{where} \quad \lambda_i = \lambda_{21}(1+z_i). \quad (17)$$

For the next-generation SKAO-MID, we follow the SKAO Cosmology Red Book (SKA Collaboration, 2020) and use $N_{\text{dish}} = 197$, $D_{\text{dish}} = 15$ m, $t_{\text{tot}} = 10^4$ hr, observing over $20,000 \text{ deg}^2$ in the redshift range $0.35 \leq z \leq 3.05$ ($1050 \geq \nu \geq 350$ MHz, Band 1). We divide the redshift range into 27 tomographic bins with width 0.1. The cleaning of foregrounds from the HI intensity map effectively removes the largest scales, $\ell \lesssim 5$ (Witzemann et al. 2019; Cunningham et al. 2019), and we take $\ell_{\min} = 5$.

3.2 Radio survey: interferometer mode

For interferometer-mode intensity mapping, the noise is (Bull et al. 2015; Alonso et al. 2017; Cosmic Visions 21 cm, 2018; Durrer et al. 2020; Jolicoeur et al. 2021)

$$N_\ell^{\Delta HI}(v_i) = \frac{4\pi f_{\text{sky}} T_{\text{sys}}^2(v_i)}{2N_{\text{dish}} t_{\text{tot}} \Delta v} \frac{\theta_{\text{FWHM}}^2(\lambda_i)}{\eta^2 N_b (\ell \lambda_i / (2\pi)) \lambda_i^2}, \quad (18)$$

$$T_{\text{sys}}(v_i) = \bar{T}_{\text{ampl}} + \bar{T}_{\text{ground}} + T_{\text{sky}}, \quad (19)$$

where $\eta = 0.7$ is the aperture efficiency factor, N_b is the density of baselines in the image plane, $\bar{T}_{\text{ampl}} = 61.73$ K is the amplifier noise temperature corrected by the optical efficiency, $\bar{T}_{\text{ground}} = 33.33$ K is due to the fraction of primary beam hitting the ground, and

$$T_{\text{sky}}(v_i) = 2.7 + 25 \left(\frac{400 \text{ MHz}}{v_i} \right)^{2.75} \text{ K}. \quad (20)$$

For the futuristic PUMA experiment, we follow Cosmic Visions 21 cm, (2018); PUMA Collaboration, (2019) and assume $N_{\text{dish}} = 32,000$ dishes arranged in hexagonal close-packed array with 50% fill factor, $D_{\text{dish}} = 6$ m, an integration time of $t_{\text{tot}} = 4 \times 10^4$ hr, observing over half of the sky ($f_{\text{sky}} = 0.5$) in the redshift range $0.3 \leq z \leq 6$. We divide the redshift range into 57 tomographic bins with width 0.1. As for SKAO, we take $\ell_{\min} = 5$.

3.3 Optical survey

For a next-generation photometric galaxy survey similar to the Vera C. Rubin Observatory’s Legacy Survey of Space and Time (LSST), we assume a redshift distribution of sources of the form

$$\bar{n}_g(z) \propto z^\alpha \exp \left[-\left(\frac{z}{z_0} \right)^\beta \right] \text{ gal/arcmin}^2. \quad (21)$$

The distribution of sources in the i -th redshift bin, including photometric uncertainties, following Ma et al. (2005), is

$$n_g^i(z) = \int_{z_{\text{ph}}^i}^{z_{\text{ph}}^{i+1}} dz_{\text{ph}} \bar{n}_g(z) p(z_{\text{ph}}|z), \quad (22)$$

where we adopt a Gaussian distribution for the probability distribution of photometric redshift estimates z_{ph} , given true redshifts z :

$$p(z_{\text{ph}}|z) = \frac{1}{\sqrt{2\pi} \sigma_z} \exp \left[-\frac{(z - z_{\text{ph}})^2}{2\sigma_z^2} \right]. \quad (23)$$

The shot noise for galaxies in the i -th redshift bin is the inverse of the angular number density of galaxies:

$$\mathcal{N}_\ell^{gi} = \left(\int dz n_g^i(z) \right)^{-1}. \quad (24)$$

For LSST clustering measurements, we assume a total number density of galaxies of $\bar{n}_g = 48$ sources per arcmin 2 , observed over 13,800 deg 2 and distributed in redshift according to (21), with $\alpha = 2$, $\beta = 0.9$, and $z_0 = 0.28$, corresponding to the Y10 gold sample ($i_{\text{lim}} = 25.3$) specifications from LSST Dark Energy Science Collaboration, (2018). We assume 10 tomographic bins spaced by 0.1, in the range $0.2 \leq z \leq 1.2$, with photometric redshift uncertainties $\sigma_z = 0.03(1+z)$. The fiducial model for the bias is $b_g(z) = 0.95/D(z)$, where D is the growth factor (LSST Dark Energy Science Collaboration, 2018). We impose $\ell_{\text{min}} = 20$.

3.4 Microwave survey

We work with a possible CMB-S4 configuration assuming a 3 arcmin beam and $\sigma_T^{1/2} = \sigma_P^{1/2}/\sqrt{2} = 1 \mu\text{K}\text{-arcmin}$ noise (CMB-S4 Collaboration, 2016). We assume $\ell_{\text{min}} = 30$ and a different cut at high- ℓ of $\ell_{\text{max}}^T = 3000$ in temperature and $\ell_{\text{max}}^P = 5000$ in polarization, with $f_{\text{sky}} = 0.4$.

For CMB temperature and polarization angular power spectra, the instrumental noise deconvolved with the instrumental beam is defined by (Knox 1995)

$$\mathcal{N}_\ell^{\text{T,P}} = \sigma_{\text{T,P}} B_\ell^{-2}, \quad (25)$$

where the Gaussian beam is given by (16).

For CMB lensing, we assume that the lensing reconstruction can be performed with the minimum variance quadratic estimator on the full sky, combining the TT, EE, BB, TE, TB, and EB estimators, calculated according to Hu & Okamoto (2002) with quicklens¹⁰ and applying iterative lensing reconstruction (Hirata & Seljak 2003; Smith et al. 2012). We use the CMB-S4 lensing information in the range $30 \leq \ell \leq 3000$.

We will refer to the full set of CMB information including temperature, E-mode polarization, CMB lensing, and their cross-correlations, as simply ‘CMB’.

4 CORRELATION BETWEEN CMB LENSING AND LARGE-SCALE STRUCTURE

The performance of the cross-correlation analysis depends on the cross-correlation coefficient. This is similar to the signal-to-noise ratio in each redshift bin (Ballardini & Maartens 2019), but without taking into account the number of modes and the sky fraction:

$$r_\ell^{X\phi}(z_i) = \frac{|C_\ell^{X\phi}(z_i)|}{[\Gamma_\ell^{XX}(z_i) \Gamma_\ell^{\phi\phi}]^{1/2}}, \quad (26)$$

where $X = \text{HI}$ or g . Figure 2 shows the correlation coefficient of SKAO-MID, PUMA redshift bins with CMB lensing expected from CMB-S4. The grey shading for $\ell < 30$ is the region where we do not have cross-correlation with CMB-S4.

The cross-correlation reaches a maximum at low redshift and it drops on small scales. Moving toward higher redshift, the correlation

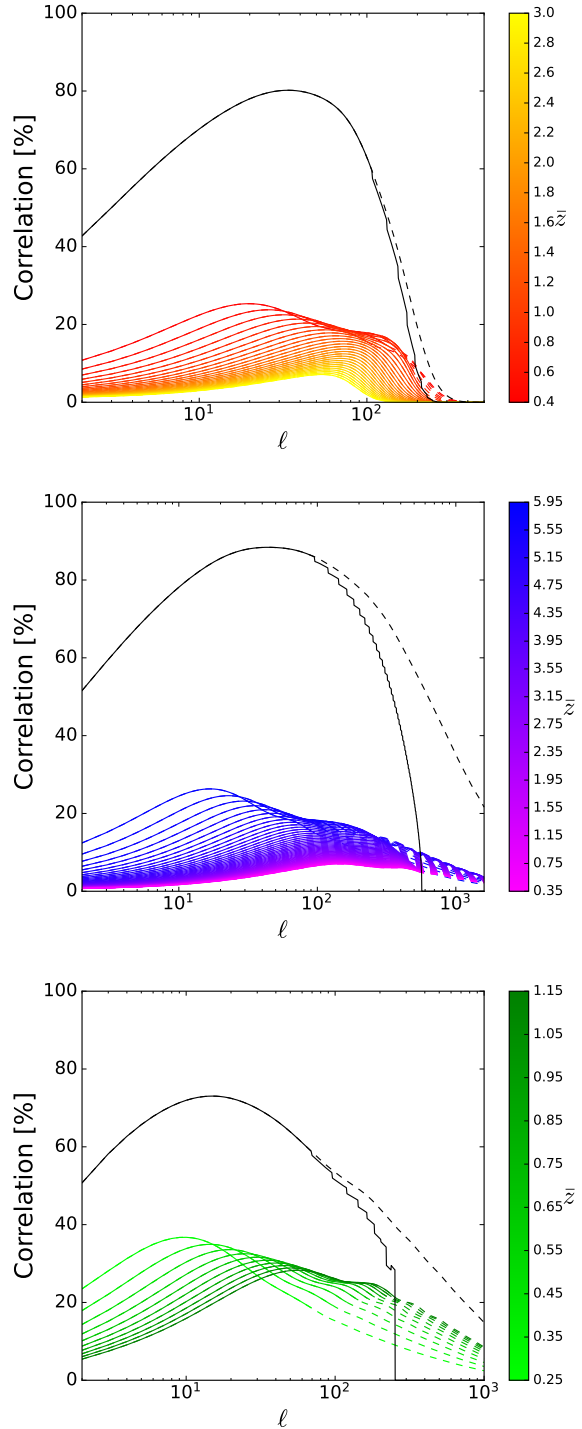


Figure 2. Expected correlation coefficient (26) between CMB-S4 lensing and SKAO-MID redshift bins (top), PUMA redshift bins (centre), and LSST photometric redshift bins (bottom). Black line shows the combined coefficient. Dashed lines denote the correlation coefficient calculated without imposing the cut of non-linear scales corresponding to $\ell(z) \sim 0.1 h\chi(z)$.

¹⁰ <https://github.com/dhanson/quicklens>

peaks at higher multipoles. This is connected to the position of the peak of the matter power spectrum in Fourier space at $k_{\text{peak}} \sim 0.02 h/\text{Mpc}$, which is mapped to higher multipoles for higher redshift according to $\ell_{\text{peak}}(z) \simeq k_{\text{peak}} \chi(z)$ where $\chi(z)$ is the comoving radial distance.

The correlation coefficient and in particular the one obtained combining the tomographic redshift bins (black line in Figure 2) can be maximised by optimising the size and edges of the redshift bins. Choosing these weights such that they maximise the correlation coefficient between the joint analyses can be used to maximise the effect of sample variance cancellation.

Combining together the information from all redshift bins for each multipole, we can define the correlation coefficient (Sherwin & Schmittfull 2015)

$$r_{\ell}^{X\phi} = \left\{ \sum_{i,j} r_{\ell}^{X\phi}(z_i) [r_{\ell}^{XX}]^{-1}(z_i, z_j) r_{\ell}^{X\phi}(z_j) \right\}^{1/2} \quad (27)$$

where

$$r_{\ell}^{XX}(z_i, z_j) = \frac{C_{\ell}^{XX}(z_i, z_j)}{\Gamma_{\ell}^{XX}(z_i, z_j)}. \quad (28)$$

The combined cross-correlation coefficient for SKAO-MID and PUMA is higher ($\sim 90\%$ at $\ell \sim 50$) in the region of interest compared to LSST. This is due to the wider redshift range probed by the IM surveys compared to photometric surveys. Note that the cross-correlation coefficient for SKAO-MID drops at $\ell \sim 200$ because of the telescope beam (16).

5 RESULTS

We present in this section the uncertainties on the total neutrino mass M_{ν} for different combinations of cosmological surveys and considering a conservative $k_{\text{max}} = 0.1 h/\text{Mpc}$, so that we consider on scales where linear perturbation theory is reliable. (Note that for SKAO-MID, the telescope beam effectively removes scales $k > 0.1 h/\text{Mpc}$). This k -cut is propagated to angular modes through the relation $\ell(z) \sim k\chi(z)$.

Note that CMB-S4 with $\ell_{\text{min}} = 30$ delivers $\sigma(M_{\nu}) \simeq 115 \text{ meV}$ while complementing the low- ℓ down to $\ell_{\text{min}} = 2$ with LiteBIRD, it can reach $\sigma(M_{\nu}) \simeq 38 \text{ meV}$.

Uncertainties are marginalised over all 6 standard cosmological parameters in (10). We also marginalise over the nuisance parameters that allow for a free redshift evolution of the clustering bias b_g , or of the combination $T_{\text{HI}} b_{\text{HI}}$ for IM, and the magnification bias s_g , for each redshift bin. This leads to 27 temperature-bias parameters for SKAO-MID, 57 temperature-bias parameters for PUMA, 10 clustering bias parameters and 10 magnification bias parameters for the LSST survey.

The uncertainties for the single surveys with SKAO-MID, PUMA and LSST are large compared to the fiducial assumption of $M_{\nu} = 60 \text{ meV}$, as shown in Table 1. Single-tracer results do improve when the scale-dependent bias is included, but the major improvement comes from the multi-tracer. Including CMB information from CMB-S4 with $\ell_{\text{min}} = 30$, using the multi-tracer, delivers:

$$\sigma(M_{\nu}) \simeq \begin{cases} 45 \text{ meV} & \text{SKAO-MID} \times \text{CMB-S4}, \\ 26 \text{ meV} & \text{PUMA} \times \text{CMB-S4}, \\ 62 \text{ meV} & \text{LSST} \times \text{CMB-S4}, \end{cases} \quad (29)$$

for $k_{\text{max}} = 0.1 h/\text{Mpc}$, while the combination of IM and LSST leads

	$\sigma(M_{\nu}) [\text{meV}]$	
	without bias	with bias
SKAO-MID	266	234
PUMA	76	77
LSST	846	782
SKAO-MID \times CMB-S4	47	45
PUMA \times CMB-S4	30	26
LSST \times CMB-S4	69	62
SKAO-MID \times LSST	240	118
PUMA \times LSST	59	54

Table 1. Two-tracer case. Marginalised uncertainties on M_{ν} at 68% CL including (right column) or neglecting (left column) the scale-dependent halo bias induced by massive neutrinos. Uncertainties are for $k_{\text{max}} = 0.1 h/\text{Mpc}$.

	$\sigma(M_{\nu}) [\text{meV}]$	
	without bias	with bias
SKAO-MID \times LSST + CMB-S4	73	63
SKAO-MID \times LSST \times CMB-S4	17	12
PUMA \times LSST + CMB-S4	28	28
PUMA \times LSST \times CMB-S4	12	11

Table 2. As in Table 1, for the three-tracer case.

to

$$\sigma(M_{\nu}) \simeq \begin{cases} 118 \text{ meV} & \text{SKAO-MID} \times \text{LSST}, \\ 54 \text{ meV} & \text{PUMA} \times \text{LSST}. \end{cases} \quad (30)$$

When all three tracers are combined, the tightest constraints obtained are

$$\sigma(M_{\nu}) \simeq \begin{cases} 12 \text{ meV} & \text{SKAO-MID} \times \text{LSST} \times \text{CMB-S4}, \\ 11 \text{ meV} & \text{PUMA} \times \text{LSST} \times \text{CMB-S4}, \end{cases} \quad (31)$$

for $k_{\text{max}} = 0.1 h/\text{Mpc}$.

We present the three-tracer case in Table 2. Adding CMB-S4 information to the multi-tracer combination of SKAO-MID and LSST reduces the error by a factor ~ 2 , to 63 meV. However, if we include all cross-correlations – between the CMB fields, intensity mapping and number counts – then the error is reduced by a factor ~ 5 , to 12 meV. This effect is completely due to the cross-correlation with the CMB lensing ϕ : neglecting the cross-correlation with E and T, we found the change in the uncertainties on the neutrino mass to be less than 1% in all cases. Figure 3 shows the marginalized uncertainties on the 3-dimensional $(\Omega_{m,0}, H_0, M_{\nu})$ parameter space.

As already shown in Brinckmann et al. (2019); Yu et al. (2018), the addition of extra constraints on the optical depth τ_{reio} at recombination can reduce further the uncertainties on the neutrino mass, breaking the partial degeneracy between M_{ν} and the normalization of the anisotropy $A_s \exp(-2\tau_{\text{reio}})$. We present in Table 3 the uncertainties on M_{ν} obtained when adding a Gaussian prior of $\sigma(\tau_{\text{reio}}) = 0.008$, corresponding to current constraints from Planck (Planck Collaboration, 2020b). We also consider $\sigma(\tau_{\text{reio}}) = 0.001$, which is possible with future CMB cosmic-variance polarisation experiments, or using independent information from 21cm IM (Liu et al. 2016).

Note that, considering our agnostic assumption about bias parameters any additional information regarding the clustering bias would improve the constraints on the neutrino mass. By contrast,

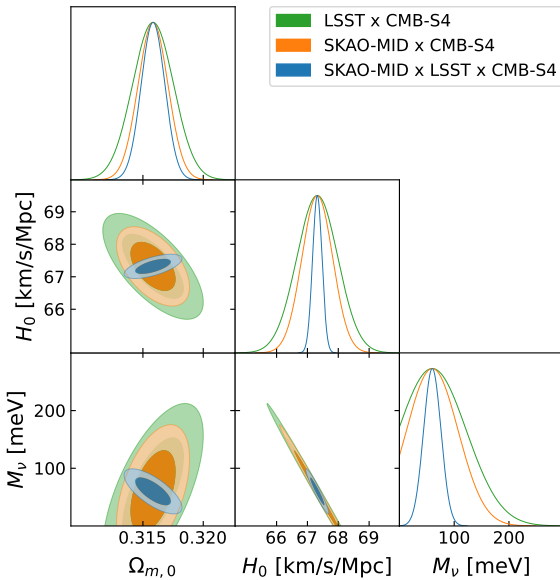


Figure 3. Marginalised 2-dimensional contours (68% and 95% CL) for $\Omega_{m,0}$, H_0 , M_ν . The multi-tracer combinations are: LSST x CMB-S4 (green), SKAO-MID x CMB-S4 (orange), and SKAO-MID x LSST x CMB-S4 (blue).

$\sigma(M_\nu)$ [meV]		
$\sigma(\tau_{\text{reio}})$	0.008	0.001
SKAO-MID x LSST x CMB-S4	14	11
PUMA x LSST x CMB-S4	11	9

Table 3. As in Table 2, including the scale-dependent halo bias in combination with a Gaussian prior on τ_{reio} .

marginalisation over magnification bias does not significantly affect uncertainties on neutrino mass.

Finally, we find that modelling the scale-dependent features in the clustering bias due to the presence of massive neutrinos reduces the uncertainties significantly for the single-tracer cases, but for the multi-tracer cases there is only a slight improvement for such a small choice of $M_\nu = 60$ meV.

6 CONCLUSIONS

We presented Fisher forecast constraints on the total neutrino mass from upcoming 21cm intensity mapping and photometric galaxy surveys, together with CMB lensing, temperature and polarisation data. We included the scale-dependent clustering bias that is induced by neutrinos. The critical feature of our analysis was to use a multi-tracer analysis that combined all the information, leading to significant improvements over single-tracer constraints or the simple addition of separate Fisher information for single tracers. The best results are achieved with a 3-tracer combination of 21cm intensity mapping, photometric survey and CMB.

Constraints on the neutrino mass have been extensively studied; see e.g. Hall & Challinor (2012); Allison et al. (2015); Villaescusa-Navarro et al. (2015); Schmittfull & Seljak (2018); Brinckmann et al. (2019); Yu et al. (2018); Boyle (2019); Archidiacono et al. (2020); Xu et al. (2021); Tanidis & Camera (2021); Bermejo-Climent et al.

(2021); Sailer et al. (2021); Bayer et al. (2021). While the combination of CMB and large-scale structure measurements is very powerful in breaking the geometrical degeneracy at background level, cosmological constraints depend strongly on the CMB low- ℓ measurements. Uncertainties of $\sigma(M_\nu) \simeq 20 - 30$ meV, corresponding to a 2-3 σ detection for a minimum neutrino mass $M_\nu = 60$ meV, have been forecast when combining CMB anisotropies and future survey number counts, and including the *Planck* constraint $\sigma(\tau_{\text{reio}}) \simeq 0.008$ on reionisation (Planck Collaboration, 2020b). These uncertainties are robust for extensions of the Λ CDM concordance model, such as cosmologies where also N_{eff} and the dark energy parameters are varied (Brinckmann et al. 2019; Boyle 2019). Moreover, the combination of different late-time probes such as BAO, galaxy clustering, galaxy weak lensing, and CMB weak lensing allows robust constraints without including any information regarding τ_{reio} (Brinckmann et al. 2019; Boyle 2019; Xu et al. 2021).

However, smaller uncertainties of the order of $\sigma(M_\nu) \simeq 10$ meV have been predicted only in combination with a tighter constraint on the optical depth at recombination $\sigma(\tau_{\text{reio}}) \simeq 0.001 - 0.002$ (Brinckmann et al. 2019; Yu et al. 2018).

Using a three-tracer approach that combines clustering measurements from two next-generation large-scale structure surveys together with CMB-S4 measurements, we showed that if only linear scales are included, the 21cm intensity mapping surveys outperform the photometric LSST survey.

The multi-tracer combination of CMB-S4 with intensity mapping delivers

$$\sigma(M_\nu) \simeq \begin{cases} 45 \text{ meV} & \text{SKAO-MID} \times \text{CMB-S4}, \\ 26 \text{ meV} & \text{PUMA} \times \text{CMB-S4}, \end{cases} \quad (32)$$

for $k_{\text{max}} = 0.1 h/\text{Mpc}$, and when marginalising over 6 standard cosmological parameters and over all nuisance parameters (27 for SKAO-MID and 57 for PUMA). These results are not sensitive to increasing ℓ_{min} up to 20 since the extra constraining power comes from the cross-correlation between CMB lensing with intensity mapping.

When all three tracers are included in a multi-tracer analysis, the tightest uncertainties predicted are

$$\sigma(M_\nu) \simeq 12/11 \text{ meV} \text{ SKAO-MID/PUMA} \times \text{LSST} \times \text{CMB-S4}. \quad (33)$$

Improved constraints in the linear regime can be obtained if we assume a prior on the reionisation optical depth (see Table 3).

In Chen et al. (2021) the 1-loop power spectrum (allowing an increase in k_{max}) and the tree-level bispectrum are used to significantly improve constraints from the cross-correlation of LSST and CMB-S4 (see also Chudaykin & Ivanov 2019; Kamalinejad & Slepian 2020; Hahn & Villaescusa-Navarro 2021, for galaxy bispectrum constraints on M_ν). Here we have avoided the complexities of going beyond linear modelling, relying instead on the multi-tracer combination of the first-order power spectra of two large-scale structure surveys together with CMB.

ACKNOWLEDGEMENTS

MB acknowledges financial contribution from the contract ASI/INAF for the Euclid mission n.2018-23-HH.0. RM is supported by the South African Radio Astronomy Observatory (SARAO) and the National Research Foundation (Grant No. 75415) and by the UK STFC Consolidated Grant ST/S000550/1.

DATA AVAILABILITY

The data underlying this article will be shared on reasonable request to the corresponding author.

REFERENCES

- Allison R., Caucal P., Calabrese E., Dunkley J., Louis T., 2015, *Phys. Rev. D*, 92, 123535
- Alonso D., Ferreira P. G., 2015, *Phys. Rev.*, D92, 063525
- Alonso D., Bull P., Ferreira P. G., Maartens R., Santos M., 2015, *Astrophys. J.*, 814, 145
- Alonso D., Ferreira P. G., Jarvis M. J., Moodley K., 2017, *Phys. Rev. D*, 96, 043515
- Archidiacono M., Hannestad S., Lesgourgues J., 2020, *JCAP*, 09, 021
- BOSS Collaboration, 2017, *Mon. Not. Roy. Astron. Soc.*, 470, 2617
- Ballardini M., Maartens R., 2019, *Mon. Not. Roy. Astron. Soc.*, 485, 1339
- Ballardini M., Mathewson W. L., Maartens R., 2019, *Mon. Not. Roy. Astron. Soc.*, 489, 1950
- Ballardini M., Braglia M., Finelli F., Paoletti D., Starobinsky A. A., Umiltà C., 2020, *JCAP*, 10, 044
- Bardeen J. M., Bond J., Kaiser N., Szalay A., 1986, *Astrophys. J.*, 304, 15
- Bayer A. E., Banerjee A., Seljak U., 2021, Beware of Fake vs: The Effect of Massive Neutrinos on the Non-Linear Evolution of Cosmic Structure ([arXiv:2108.04215](#))
- Bermejo-Clement J. R., Ballardini M., Finelli F., Paoletti D., Maartens R., Rubiño Martín J. A., Valenziano L., 2021, *Phys. Rev. D*, 103, 103502
- Bird S., Viel M., Haehnelt M. G., 2012, *Mon. Not. Roy. Astron. Soc.*, 420, 2551
- Boyle A., 2019, *JCAP*, 1904, 038
- Brinckmann T., Hooper D. C., Archidiacono M., Lesgourgues J., Sprenger T., 2019, *JCAP*, 1901, 059
- Bull P., Ferreira P. G., Patel P., Santos M. G., 2015, *Astrophys. J.*, 803, 21
- CMB-S4 Collaboration, 2016. ([arXiv:1610.02743](#))
- Castorina E., Sefusatti E., Sheth R. K., Villaescusa-Navarro F., Viel M., 2014, *JCAP*, 02, 049
- Challinor A., Lewis A., 2011, *Phys. Rev.*, D84, 043516
- Chen S.-F., Lee H., Dvorkin C., 2021, *JCAP*, 05, 030
- Chiang C.-T., Hu W., Li Y., Loverde M., 2018, *Phys. Rev. D*, 97, 123526
- Chiang C.-T., LoVerde M., Villaescusa-Navarro F., 2019, *Phys. Rev. Lett.*, 122, 041302
- Chudaykin A., Ivanov M. M., 2019, *JCAP*, 11, 034
- Coles P., 1993, *Monthly Notices of the Royal Astronomical Society*, 262, 1065
- Cosmic Visions 21 cm, 2018. ([arXiv:1810.09572](#))
- Cunnington S., Wolz L., Pourtsidou A., Bacon D., 2019, *Mon. Not. Roy. Astron. Soc.*, 488, 5452
- Di Valentino E., Gariazzo S., Mena O., 2021, *Phys. Rev. D*, 104, 083504
- Durrer R., Jalilvand M., Kothari R., Maartens R., Montanari F., 2020, *JCAP*, 12, 003
- Eisenstein D. J., Hu W., 1997, *Astrophys. J.*, 511, 5
- Fonseca J., Camera S., Santos M., Maartens R., 2015, *Astrophys. J.*, 812, L22
- Hahn C., Villaescusa-Navarro F., 2021, *JCAP*, 04, 029
- Hall A. C., Challinor A., 2012, *Mon. Not. Roy. Astron. Soc.*, 425, 1170
- Hannestad S., 2006, *Ann. Rev. Nucl. Part. Sci.*, 56, 137
- Hirata C. M., Seljak U., 2003, *Phys. Rev.*, D68, 083002
- Howlett C., Lewis A., Hall A., Challinor A., 2012, *JCAP*, 1204, 027
- Hu W., Eisenstein D. J., 1998, *Astrophys. J.*, 498, 497
- Hu W., Okamoto T., 2002, *Astrophys. J.*, 574, 566
- Hu W., White M. J., 1997, *Phys. Rev.*, D56, 596
- Ivanov M. M., Simonović M., Zaldarriaga M., 2020, *Phys. Rev. D*, 101, 083504
- Jolicoeur S., Maartens R., De Weerd E. M., Umeh O., Clarkson C., Camera S., 2021, *JCAP*, 06, 039
- Kaiser N., 1984, *Astrophys. J. Lett.*, 284, L9
- Kamalinejad F., Slepian Z., 2020. ([arXiv:2011.00899](#))
- Knox L., 1995, *Phys. Rev. D*, 52, 4307
- LSST Dark Energy Science Collaboration, 2018. ([arXiv:1809.01669](#))
- Lattanzi M., Gerbino M., 2018, *Front. in Phys.*, 5, 70
- Lesgourgues J., Pastor S., 2006, *Phys. Rept.*, 429, 307
- Lesgourgues J., Pastor S., 2012, *Adv. High Energy Phys.*, 2012, 608515
- Lewis A., Challinor A., Lasenby A., 2000, *Astrophys. J.*, 538, 473
- Liu A., Pritchard J. R., Allison R., Parsons A. R., Seljak U., Sherwin B. D., 2016, *Phys. Rev. D*, 93, 043013
- LoVerde M., 2014, *Phys. Rev. D*, 90, 083530
- LoVerde M., 2016, *Phys. Rev. D*, 93, 103526
- Ma Z.-M., Hu W., Huterer D., 2005, *Astrophys. J.*, 636, 21
- Mann B., Peacock J., Heavens A., 1998, *Mon. Not. Roy. Astron. Soc.*, 293, 209
- MeerKCLASS Collaboration, 2017, in Proceedings, MeerKAT Science: On the Pathway to the SKA 2016. ([arXiv:1709.06099](#))
- PUMA Collaboration, 2019, *Bull. Am. Astron. Soc.*, 51, 53
- Planck Collaboration, 2020a, *Astron. Astrophys.*, 641, A1
- Planck Collaboration, 2020b, *Astron. Astrophys.*, 641, A6
- Planck Collaboration, 2020c, *Astron. Astrophys.*, 641, A8
- Raccanelli A., Verde L., Villaescusa-Navarro F., 2019, *Mon. Not. Roy. Astron. Soc.*, 483, 734
- Roy Choudhury S., Hannestad S., 2020, *JCAP*, 07, 037
- SKA Collaboration, 2020, *Publ. Astron. Soc. Austral.*, 37, e007
- Sailer N., Castorina E., Ferraro S., White M., 2021. ([arXiv:2106.09713](#))
- Schmittfull M., Seljak U., 2018, *Phys. Rev.*, D97, 123540
- Sekiguchi T., Takahashi T., 2021, *Phys. Rev. D*, 103, 083516
- Seljak U., 2009, *Phys. Rev. Lett.*, 102, 021302
- Sherwin B. D., Schmittfull M., 2015, *Phys. Rev. D*, 92, 043005
- Smith K. M., Hanson D., LoVerde M., Hirata C. M., Zahn O., 2012, *JCAP*, 1206, 014
- Sprenger T., Archidiacono M., Brinckmann T., Clesse S., Lesgourgues J., 2019, *JCAP*, 02, 047
- Takahashi R., Sato M., Nishimichi T., Taruya A., Oguri M., 2012, *Astrophys. J.*, 761, 152
- Tanidis K., Camera S., 2021, *Mon. Not. Roy. Astron. Soc.*, 502, 2952
- Vagnozzi S., Giusarma E., Mena O., Freese K., Gerbino M., Ho S., Lattanzi M., 2017, *Phys. Rev. D*, 96, 123503
- Vagnozzi S., Brinckmann T., Archidiacono M., Freese K., Gerbino M., Lesgourgues J., Sprenger T., 2018, *JCAP*, 09, 001
- Villaescusa-Navarro F., Marulli F., Viel M., Branchini E., Castorina E., Sefusatti E., Saito S., 2014, *JCAP*, 03, 011
- Villaescusa-Navarro F., Bull P., Viel M., 2015, *Astrophys. J.*, 814, 146
- Witzemann A., Alonso D., Fonseca J., Santos M. G., 2019, *Mon. Not. Roy. Astron. Soc.*, 485, 5519
- Wong Y. Y. Y., 2011, *Ann. Rev. Nucl. Part. Sci.*, 61, 69
- Xu W. L., DePorzio N., Muñoz J. B., Dvorkin C., 2021, *Phys. Rev. D*, 103, 023503
- Yu B., Knight R. Z., Sherwin B. D., Ferraro S., Knox L., Schmittfull M., 2018. ([arXiv:1809.02120](#))